An improved satellite-based evapotranspiration routine for China

Lei Huang[1], Yong Luo[1], Tammo S Steenhuis[2], Qiuhong Tang[3], Wei Cheng[4], Wen Shi[1], Xin Xia[1], Lihua Zhou[1], and Zhouyi Liao[1]

[1]Tsinghua University
[2]Cornell University
[3]Institute of Geographic Sciences and Natural Resources Research, Chinese Academy of Sciences
[4]Institute of Geographic Sciences and Natural Resources Research

November 24, 2022

Abstract

Evapotranspiration (ET) is a critical process that regulates the heat and water transfer between the land and atmosphere. Instantaneous satellite data can provide area-wide daily ET measurements. Surface energy budgets used in satellite-based calculations generally overpredict daily net radiation and the related ET. Our objective was to improve the accuracy of satellite-based daily evapotranspiration by correcting the overprediction of net radiation.

To do so, we introduced a routine for calculating the downward longwave radiation on cloudy days. This new algorithm removed the upward bias in the predicted net radiation at seven ChinaFlux sites. Then, using previously developed methods for converting instantaneous measurement into daily averages, we found that evapotranspiration rates were predicted more accurately than existing methods at the same ChinaFlux sites. In addition, our evapotranspiration rates compared well with watershed ET and other calibrated and validated spatiotemporal gridded data products in China

An improved satellite-based evapotranspiration routine for China

Lei Huang[1*], Yong Luo[1*], Tammo Steenhuis[2], Qiuhong Tang[3,4], Wei Cheng[5,6], Wen Shi[1], Xin Xia[1], Lihua Zhou[1], Zhouyi Liao[1]

[1]Department of Earth System Science, Ministry of Education Key Laboratory for Earth System Modeling, Institute for Global Change Studies, Tsinghua University, Beijing 100084, China,

[2]Department of Biological and Environmental Engineering, Cornell University, Ithaca, NY, USA,

[3]Key Laboratory of Water Cycle and Related Land Surface Processes, Institute of Geographic Sciences and Natural Resources Research, Chinese Academy of Sciences, Beijing, 100101, China

[4]University of Chinese Academy of Sciences, Beijing, China,

[5]Institute of Geographic Sciences and Natural Resources Research, Chinese Academy of Sciences, Beijing, China.

[6]Key Laboratory of Land Surface Pattern and Simulation, Chinese Academy of Sciences, Beijing, China.

Corresponding authors: Lei Huang (leihuang007@mail.tsinghua.edu.cn) and Yong Luo (Yongluo@mail.tsinghua.edu.cn)

Key Points

- We improved satellite-based daily evapotranspiration calculations by introducing a procedure for downward longwave radiation on cloudy days.
- This revised downward longwave radiation procedure improved the accuracy of the daily net radiation compared with existing methods.
- Evapotranspiration calculated with the improved satellite-based routine agreed well with eddy covariance measurements and watershed studies.

Abstract

Evapotranspiration (ET) is a critical process that regulates the heat and water transfer between the land and atmosphere. Instantaneous satellite data can provide area-wide daily ET measurements. Surface energy budgets used in satellite-based calculations generally overpredict daily net radiation and the related ET. Our objective was to improve the accuracy of satellite-based daily evapotranspiration by correcting the overprediction of net radiation.

To do so, we introduced a routine for calculating the downward longwave radiation on cloudy days. This new algorithm removed the upward bias in the predicted net radiation at seven ChinaFlux sites. Then, using previously developed methods for converting instantaneous measurement into daily averages, we found that evapotranspiration rates were predicted more accurately than existing methods at the same ChinaFlux sites. In addition, our evapotranspiration rates compared well with watershed ET and other calibrated and validated spatiotemporal gridded data products in China

Plain language summary

Evaporation drives the earth's water cycle. Satellites, when passing over, provide large-scale measurements from which daily evaporation rates can be calculated. Researchers are trying to refine these calculations. We found that existing methods to estimate net radiation, a vital parameter for calculating evaporation, were generally greater than observed. Net radiation is the difference between what comes to the surface and what leaves the earth via long-wave radiation. After studying the current methods used, it appeared that the longwave radiation of clouds to the earth could be improved. We quantified this longwave radiation component as a function of the cloudiness without the need to collect additional data. When this longwave component was included in existing models, the predicted evaporation rate compared well with other more direct measurements available in space and time in China.

1. Introduction

Evapotranspiration (ET) modulates the earth's energy budget and water and carbon cycles (Miguez-Macho & Fan, 2021; Wang et al., 2014). Quantitative assessment of area-wide ET is, therefore, crucial in quantifying the historical change constraining the future climate change impact on the hydrological cycle (Kingston et al., 2009; Pascolini-Campbell et al., 2021; Teuling et al., 2013). Satellites can provide area-wide ET estimates (Tang et al., 2009; Yang et al., 2013) by extrapolating the instantaneous measurements to daily averages. Early research (Brutsaert & Sugita, 1992; Stewart et al., 1998) assumed that the instantaneous ratio of ET to the available energy was constant throughout the day (i.e., constant Evaporation fraction, EF method), leading to an underestimation of 20-30% in the daily ET (Van Niel et al., 2012; Xu et al., 2015; Yang et al., 2013). Some studies used the instantaneous ratio of extraterrestrial radiation, top-of-atmosphere radiation, or reference EF to their daily values to replace the constant EF method (Ryu et al., 2012; Cammalleri et al., 2014). However, these methods need auxiliary observed data to calculate actual ET, limiting its applicability to other sites.

A promising improvement that uses only satellite measurements was the EF method developed for cropland by Tang and Li (2017). It used the McNaughton-Jarvis and Penman-Monteith equations to differentiate between instantaneous and daily EF. Huang et al. (2021) extended this method for all types of land and resulted in ET estimates that agreed more closely with eddy covariance measurements than the traditional constant EF method. Despite being more accurate, other improvements are needed since ET was overestimated by 15-25% over ground measurements (Huang et al., 2021). Our review of published data (Kondo 1994; Nishida et al., 2003; Tang et al. 2009; Huang et al., 2021) indicated that the downward long-wave radiation was overpredicted, resulting in more energy available for evaporation than that was measured.

The objective of this study is to improve the previously developed satellite-based evapotranspiration of Huang et al. (2021) by improving the daily net radiation algorithm that includes an improved downward long-wave radiation component. The method's accuracy was tested for China by comparing the calculated daily net radiation and evaporation with observation China Flux sites. The ET estimates were also evaluated with basin-wide evapotranspiration and independent ET products.

2. Methodology

2.1 The satellite-based two-source evapotranspiration algorithm

The daily satellite-based evapotranspiration is obtained by calculating for each grid cell the evaporation from soil (ET_{soil}) and the transpiration from the vegetation (ET_{veg})

$$ET^d = f_{veg}\, ET_{veg}^d (1 - f_{veg}) ET_{soil}^d \tag{1}$$

where the superscript *d* denotes the daily value of the parameter and f_{veg} is the fraction of vegetation covering the soil surface and is calculated from the normalized vegetation index (NDVI). The daily ET values are obtained by extrapolating the instantaneous satellite measurements to determine the daily evaporation fraction (EF^d) for the soil and the plants, which is defined as the ratio of ET and viz

$$EF^d = \frac{ET^d}{Q^d} \tag{2}$$

where Q^d is the available energy (W m^{-2}). By dividing Eq. (1) with Q^d the daily evaporation fraction, EF^d for one grid cell can be expressed as:

$$EF^d = f_{veg}\, EF_{veg}^d\, (1 - f_{veg}) EF_{soil}^d \tag{3}$$

In the following two sections, we first discuss the improvements in the calculating the net radiation and then we provide an overview of converting the instantaneous satellite measurements into a EF^d.

2.2 Net radiation

Daily satellite-based net radiation, R_{n0}^d is calculated using the land surface energy balance Nishida (2003):

$$R_{n0}^d = (1 - albedo^d) R_d^d - \varepsilon_s^d \sigma T_s^{d\,4} + \varepsilon_a^d \sigma (\, T_a^d - 20)^4 \tag{4}$$

where $albedo^d$ is the daily albedo of the soil surface; R_d^d is daily incoming shortwave radiation (W m^{-2}; He et al., 2020; Yang et al., 2010); ε_s^d and ε_a^d are the daily emissivity of land surface and atmospheric; σ is the Stefan-Boltzmann constant, T_a^d is the daily near surface air temperature (K); T_s^d is the daily surface temperature (K); $\varepsilon_a^d \sigma (T_a^d - 20)^4$ is the daily downward long-wave radiation (W m^{-2}), $\varepsilon_s^d \sigma T_s^{d\,4}$ is the daily upward long-wave radiation (W m^{-2}).

The accuracy of calculating the various terms in Eq 4 was evaluated in the past. Huang et al. (2017) reported that R_d^d provided by the China Meteorology Forcing Datasets agreed well with surface measurements at seven flux tower sites in China. Similarly, the daily surface air temperature, T_a^d was very close to the measured at the flux towers (R^2>0.7; 2<RMSE<4 oK, Huang et al., 2021). Errors in MODIS T_s^d and ε_s^d data were less than1% (Li et al., 2014; Lu et al., 2018; Wang et al., 2007; Wang & Liang, 2009a). Finally, we found that instantaneous MODIS albedo measurements were nearly the same as the daily mean albedo, with an RMSE of less than 0.02 (Supplemental Material Figure S1). Despite the accuracy of the above-mentioned individual components in Eq 4, as noted above, the daily net radiation was greater than observed (Huang et al., 2021). Thus, since the downward longwave radiation is the only term not checked, this term must cause the overestimation in the net radiation.

Further analysis of the net radiation algorithm used in satellite-based ET indicated that the emissivity of the land surface and the atmosphere was equal in formulating the downward longwave radiation and assuming that atmospheric temperatures were 200 less than the near-surface air temperature (Kondo et al., 1994; 2000). It implied that downward longwave radiation was independent of the cloud cover, contrary to findings of Alados et al. (2012), Goforth et al. (2002), Vall & Castell, (2017) and Wang & Dickinson (2013).

2.3 Longwave radiation

The cloud cover in the downward longwave radiation term in Eq 4 was included in the work of Goforth et al. (2002) and Chang & Zhang. (2019). Without their empirical humidity terms and using their work, the net solar radiation (Eq 4) can be written as:

$$R_n^d = (1 - albedo^d)R_d^d - \varepsilon_s^d \sigma T_s^{d\,4} + \ (1 + Cloud^d)\varepsilon_a^d \sigma\, T_a^{d\,4} \qquad (5)$$

where $\varepsilon_a^d \sigma\, T_a^{d\,4}$ is the atmospheric downward longwave radiation under clear sky conditions and $Cloud^d$ is the cloud cover.

Under a clear sky and a standard humidity and temperature profile, Brutsaert, (1975) predicted the atmospheric emissivity as

$$\varepsilon_a^d = 1.24\ \times (e_a^d / T_a^d)^{1/7} \qquad (6)$$

where e_a^d is the daily water vapor pressure (kPa). Eq 6 was more accurate than those developed by Idso, 1981 and Prata, (1996), according to Kaicun Wang and Dickinson (2013) and Kaicun Wang & Liang (2009b)

The $Cloud^d$parameter in Eq 5 can be derived from the clearness index K_t (Chang & Zhang, 2019; Goforth et al., 2002).

$$Cloud = (1 - K_t) \qquad (7)$$

where

$$K_t = \frac{R_d^d}{R_a^d} \qquad (8)$$

R_a^d is the daily extraterrestrial radiation (FAO 1998):

$$R_a^d = \frac{24 \times (3600)}{\pi}\ G_{sc} d_r (\omega_s \sin(\varphi) \sin(\delta) + \cos(\varphi)\, cons(\delta) \sin(\omega_s)) \qquad (9)$$

where the G_{sc} is the solar constant, which is 1367 W m^{-2}; d_r is the distance between the earth and the Sun (m); ω_s is the sunset hour angle (rad), φ is the latitude (rad), δ is the solar decimation (rad).

2.4 Overview of the evaporation fraction

Many methods are available to convert the instantaneous measurements to daily $EF^{\ d}$ (Alfieri et al., 2017; Sobrino et al., 2007; Tang et al., 2013; Van Niel et al., 2012). In this manuscript, we follow a time-transient EF approach that was more accurate than the original Nishida et al. (2003) method (Huang et al., 2021). It is based on the McNaughton-Jarvis and Penman-Monteith equations (Huang et al., 2021) :

$$EF_{veg}^{d} = \frac{\alpha\,\Delta^{i}}{\Delta^{i}+\gamma\left(1+\frac{r_{c\,veg}^{i}}{2r_{a\,veg}^{i}}\right)}\left(\frac{\Delta^{d}}{\Delta^{d}+\gamma}\,\frac{\Delta^{i}+\gamma}{\Delta^{i}}\,\frac{\Omega_{veg}^{*\,i}}{\Omega_{veg}^{*\,d}}\,\frac{\Omega_{veg}^{d}}{\Omega_{veg}^{i}}\right) \tag{10}$$

$$EF_{soil}^{d} = \frac{T_{soil\,max}^{\,i}-T_{soil}^{\,i}}{T_{soil\,max}^{\,i}-T_{a}^{\,i}}\,\frac{Q_{soil\,0}^{\,i}}{Q_{soil}^{\,i}}\left(\frac{\Delta^{d}}{\Delta^{d}+\gamma}\,\frac{\Delta^{i}+\gamma}{\Delta^{i}}\,\frac{\Omega_{soil}^{*\,i}}{\Omega_{soil}^{*\,d}}\,\frac{\Omega_{soil}^{\,d}}{\Omega_{soil}^{\,i}}\right) \tag{11}$$

where Ω is the decoupling factor that represents the relative contribution of radiative and the aerodynamic terms to the overall evapotranspiration (McNaughton & Jarvis, 1983), Ω_{i}^{*}, decoupling factor for wet surfaces. α, Priestley-Taylor parameter set to 1.26 (De Bruin, 1983); Δ^{i}, slope of the saturated water vapor pressure (Pa K^{-1}); γ, the psychometric constant (Pa K^{-1}); $r_{c\,veg}^{i}$, instantaneous surface resistance of the vegetation canopy (s m^{-1}); $r_{a\,veg}^{i}$, instantaneous aerodynamics resistance of the canopy (s m^{-1}); $T_{soil\,max}^{i}$ is the instantaneous maximum possible temperature of bare soil when it is dry (K); T_{soil}^{i}, instantaneous temperature of the bare soil (K); T_{a}^{i}, instantaneous air temperature; Q_{soil0}^{i}, instantaneous available energy when T_{soil}^{i} is equal to T_{a}^{i} (W m^{-2}).

2.5 Testing the method

Since daily parameters are often not accurately determined from instantaneous satellite measurements in Eqs 10-11, we used four different methods to convert instantaneous measurements into daily EF values.

(a) **The EF0 method:** the original Nishida's method (2003) assumed the instantaneous EF equals its daily value (EF0), thus, $EF_{veg\,0}^{d}$ and $EF_{soil\,0}^{d}$ can be expressed as:

$$EF^{d}_{veg\,0} = \frac{\alpha\, \Delta^{i}}{\Delta^{i} + \gamma\left(1 + \frac{r^{i}_{c\,veg}}{2 r^{i}_{a\,veg}}\right)} \tag{12}$$

$$EF^{d}_{soil\,0} = \frac{T^{i}_{soil\,max} - T^{i}_{soil}}{T^{i}_{soil\,max} - T^{i}_{a}} \frac{Q^{i}_{soil\,0}}{Q^{i}_{soil}} \tag{13}$$

The following three methods are those that provided the most accurate prediction in Huang et al., 2021)

(b) **The EFd method:** all instantaneous and daily measurements were calculated in Eq 10 and 11 without any assumptions;

(c) The **EFd1 method**: the instantaneous decoupling parameter for the wet surface was assumed to be equal to its daily value: $\Omega^{*i} = \Omega^{*d}$ in Eq 10 and 11;

(d) **The EFd2 method**: the ratio of $\Omega^{*i}\ \Omega^{d}$ and $\Omega^{*d}\ \Omega^{i}$ was assumed to be 1, e.g., $\frac{\Omega^{*i}}{\Omega^{*d}} \frac{\Omega^{d}}{\Omega^{i}} = 1$ in Eq. 10 and 11.

Based on these four methods, the daily evapotranspiration can be calculated using Eqs. 12 and 13 for the Nishida methods (ET0) and Eqs. 10 and 11 with the substitutions mentioned above, followed by Eqs. 3 and 2 for ETd, ETd1 and ETd2.

3. Data

The data used in this study include the input data for ET estimation and the data for ET evaluation.

3.1 Input data

The input data include the Land Products of Moderate Resolution Imaging Spectroradiometer (MODIS) and 3-hourly downwards shortwave radiation from the Chinese Meteorology Forcing Datasets. Detailed input data are given in Supplementary Material Table S1).

3.2 Validation ET data

Data from seven ChinaFlux network sites, which applies eddy covariance and chamber methods to measure water vapor and energy exchanges between ecosystem and atmosphere, was used for local-scale evaluation. Four calibrated and validated gridded evaporation products are used for evaluating the accuracy of the satellite-based evapotranspiration estimates with Eqs (1), (10) and (11).

The measurement data were downloaded from the seven ChinaFlux sites at http://chinaflux.org/ (Yu et al., 2006). The observed net radiation data were obtained from ground observations of the conventional HMP45C and VAISALA instruments at the location of the flux tower. The ET measurements were calculated from data collected by the open-path eddy covariance (CR10XTD, CR23XTD, and CR5000) at a frequency of 10 Hz and averaged for every 30 minutes online. The daily mean ET was aggregated by this 30-minute observed ET (Zheng et al., 2016). More details of the seven sites are in Supplementary Material Table S2.

The predicted evapotranspiration was also compared for accuracy with four gridded ET products, i.e., MOD16 (Mu et al., 2007, 2011), Advanced Very-High-Resolution Radiometer (AVHRR) ET (Zhang et al., 2009), Global Biosphere Atmosphere Fluxes (GBAF) (Jung et al., 2009, 2010), and the Variable Infiltration Capacity Macroscale Hydrologic Model (VIC) ET (Zhang et al., 2014). MOD16 and AVHRR are based on remote sensing data. The GBAF product (2001-2008) was developed with machine learning using the global eddy covariance towers observations, remote sensing measurements, and meteorological data. VIC ET estimation (2001-2012) is the calibrated simulated output of VIC model. Details of the ET products are given in Supplementary Material Table S3.

Predicted ET (ET0, ETd1, ETd2 and ETd methods) and observed ET were evaluated using the Pearson's correlation coefficient (r), Root Mean Square Error (RMSE) and relative error (Supplementary Material, Equation S1, S2, S3). We also compared ET0, ETd1, ETd2 and ETd with other independent ET products by 1) calculating the multiple-year mean of these ET gridded products and compared with VIC ET with R^2 and RMSE in 10 major and 80 sub-river basins; 2) calculating the R, RMSE and Bias for every grid cell between monthly ETd1 and MOD16 (2001 to 2013), AVHRR (2001-2006), VIC (2001-2012) and GBAF (2001-2008) ET products.

4. Results and Discussion

Measurements of downward longwave radiation were not available. We, therefore, tested first the daily net radiation that includes the longwave radiation term and for which measurements were available. Next, we compared calculated ET values with the four methods with those observed at the seven ChinaFlux sites. The China-wide comparison was achieved by comparing the calculated values with existing gridded ET data products.

4.1 Daily net radiation

Daily net radiation for the seven ChinaFlux sites was compared in Figure 1 with the calculated values (Eqs 4-9). The plots confirm that the original method (Eq 4) systematically overestimated the ground measured net radiation by 30%. Net radiation calculated with the revised technique (Eqs 5-9) were closer to the observed net radiation. The RMSE improved from 41 – 58 W m^{-2} to 26 – 46 W m^{-2} for all sites except the DangXiong (DX) site (Figure 1). The DX is located in the high elevation of Tibet (Yang et al., 2010). For this site, the aerosols (e.g., fog and clouds) are overprediction causing a lower than observed short wave radiation and consequently daily net radiation.

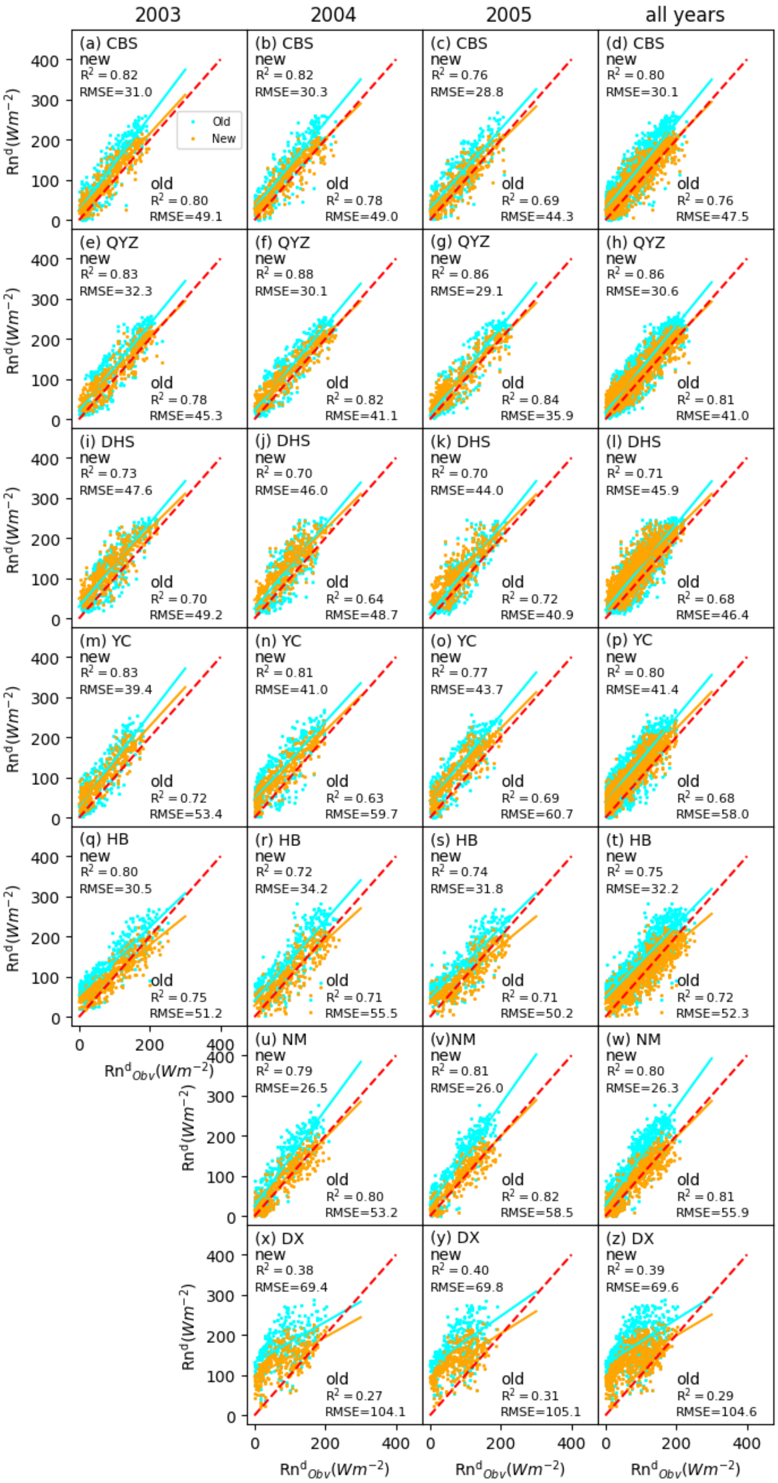

Figure 1. Scatter plots of satellite-based model simulated daily net radiation (Rn^d) plotted against the observed measurements ($Rn^d{}_{Obv}$) for an individual year and the entire 2003 to 2005 period at Changbaishan (CBS), Qianyanzhou (QYZ), Dinghushan (DHS), Yucheng (YC), Haibei (HB), Neimeng (NM), and Dangxiong (DX) sites. The blue dots are calculated with the original (old) method (Eq 4) and the orange dots with the revised (new) approach (Eqs 5-9). The red dotted line is the 1:1 line.

4.2 . Evapotranspiration

The statistical measures of the observed evapotranspiration rates for the ChinaFlux sites and the satellite-based ET0, ETd, ETd1, and EFd2 rates are in Table 1 and the scatter plots are shown in Supplementary Material Figure S2. The ET for the DX site was predicted poorly, with the four methods indicating a systematic error. It was caused by the underestimation of the daily net energy and small evaporation fraction. The latter resulted from a discrepancy in vegetation coverage, f_{veg}, between the MODIS grid cells ($f_{veg} \approx 0.1$) and the footprint of the flux tower ($f_{veg} \approx 0.3$, Huang et al., 2017). The DX site was therefore excluded from further analysis.

Comparing the four methods for calculating the ET, we note that they all overpredict the ET in CBS, QYZ and DHS sites (Supplementary Material Figure S2), which was mainly caused by the slight overestimation of R_n^d at these sites (Figure 1). ET0 had the highest R^2 among these four ET estimates, but it overestimated observed ET in CBS, QYZ, DHS and HB with relative higher RMSE. ETd1 and ETd2 were closer to the 1:1 line than ET0 (Table 1, Supplementary Material Figure S2). Thus, despite the lower R^2 in Table 1, ETd1 and ETd2 using the revised the longwave radiation procedure was more accurate. The greater accuracy of these three ET estimates was confirmed by the RMSE of 1.05 mm/day or less and relative error of 1 mm/day or less (Table 1). ETd had the weakest fit because the evaporation fraction was not calculated as accurately as ETd1 and ETd2 (Huang et al., 2021).

Table 1 The values of R^2, RMSE and relative error of ET0, ETd1, ETd2 and ETd when compared with the flux tower measurements for the entire 2003 to 2005 period at Changbaishan (CBS), Qianyanzhou (QYZ), Dinghushan (DHS), Yucheng (YC), Haibei (HB), Neimeng (NM), and Dangxiong (DX) sites.

Site name	ET0	ETd1	ETd2	ETd
		R^2		
CBS	0.78	0.75	0.78	0.67
QYZ	0.6	0.59	0.61	0.6
DHS	0.4	0.37	0.39	0.24
YC	0.59	0.56	0.56	0.53
HB	0.8	0.71	0.78	0.71
NM	0.63	0.61	0.62	0.54
Average	**0.63**	**0.60**	**0.62**	**0.55**
DX	0.62	0.57	0.62	0.42
		RMSE		
CBS	1.03	0.89	0.9	1.03
QYZ	1.26	1.15	1.19	1.26
DHS	1.95	1.37	1.85	1.94
YC	1.01	1.04	1.03	1.12
HB	0.75	0.86	0.68	0.86
NM	0.6	0.64	0.64	0.7
Average	**1.10**	**1.00**	**1.05**	**1.15**
DX	1.12	1.36	1.3	1.51
		Relative error		
CBS	0.13	-0.06	-0.03	-0.1
QYZ	0.2	0.09	0.14	0.14
DHS	0.65	0.34	0.58	0.45
YC	-0.11	-0.22	-0.19	-0.23
HB	0	-0.39	-0.26	-0.37
NM	-0.16	-0.27	-0.3	-0.29
Average	**0.12**	**-0.09**	**-0.01**	**-0.07**
DX	-0.41	-0.6	-0.56	-0.67

To judge whether our revised uncalibrated satellite-based ET0, ETd, ETd1, and EFd2 were an improvement over the existing ET products (MOD16, AVHRR and GBAF), we compared the multi-year mean ET of our four methods and three gridded ET products with those determined independently by Zhang et al. (2014) using basin water balances with ET as the rest term using the calibrated VIC model for ten major river basins and 80 sub-basins in China (Figure 2). The GRAF gridded product had the lowest RMSE and best R^2 for ten major basins and 80 subbasins for 2001-2008 (Figure 2). This was expected since all available data were used (including the potential evaporation data, precipitation data and water balance data) to obtain the GRAF evaporation rates (Jung et al., 2009, 2010). The next best performance was ETd1, followed by ETd and ETd2, with R^2 over 0.93 for the major basins and 0.87 for the subbasins. The original Nishida model had the next best accuracy, and surprisingly the two gridded MOD16 and AVHRR were in the last place.

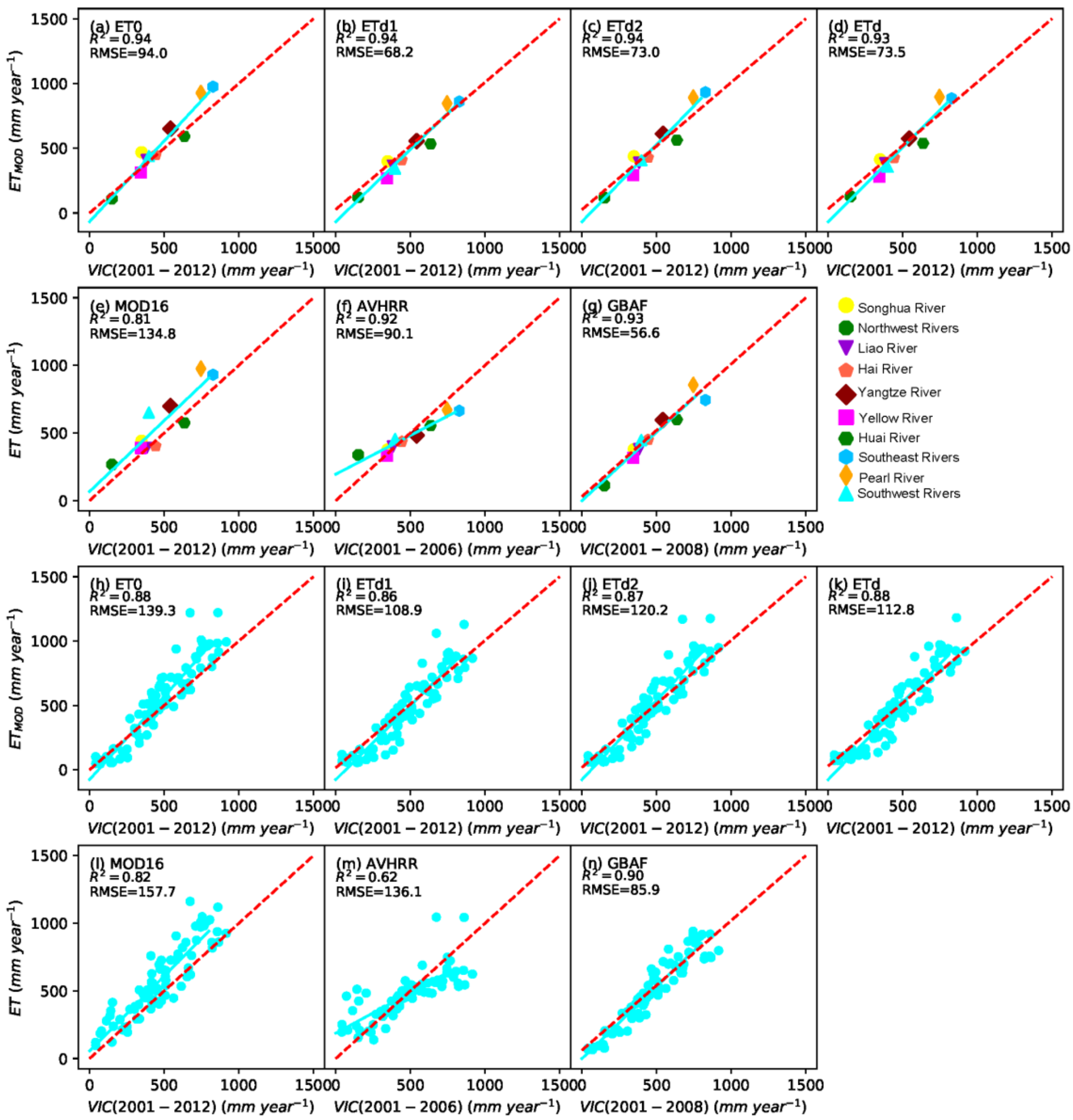

Figure 2. The Scatter plots of annual mean ET of (ET0, ETd1, ETd2, and ETd) (2001 to 2012), MOD16 (2001 to2012), AVHRR (2001 to 2006), and GBAF (2001 to 2008) against VIC at the 10 major river basins (a-g) and 80 sub-major river basins (h-n) of China during the corresponding time periods. The dotted red line is the 1:1 line, and the solid lines are the regression lines. R^2 and RMSE values over these periods are given in the plots.

To investigate where spatially our approach diverged from the existing methods, we calculated the RMSE of each grid cell's monthly averages ET values over the period ranging from 2001 to 2020 years between the four methods and the four data products (Figure 3).

The Root Mean Square Error (RMSE) of ET0, ETd1, ETd2 and ETd with other four ET products were between 15-20 mm month^{-1} in most of China except in the west and southern China, where the RMSE was greater than 30 mm month^{-1}. ETd1 has the lowest RMSE than ET0, ETd2 and ETd with RMSE between 10-15 mm month^{-1} in North China and greater than 20 mm month^{-1} in South and West China. This confirmed that ETd1 was closest to the other independent ET products. The R^2 between ET0, ETd1, ETd2 and ETd with other four ET products were relatively high (R^2>0.7) which suggested these four ET simulations had consistent spatial and temporal variation between other four independent ET products (Supplementary Material Figure S3). The Bias of ETd1 with the other products was consistently more than 20 mm month^{-1} in West China, especially Tibet (Supplementary Material Figure S4). One reason is the underestimation of daily net radiation, the other reason is the low NDVI index cause the underestimation of *fveg*; another reason is our model has limited ability of describing the evaporation on a frozen surface especially in the Qinghai-Tibet Plateau (Tang et al., 2009).

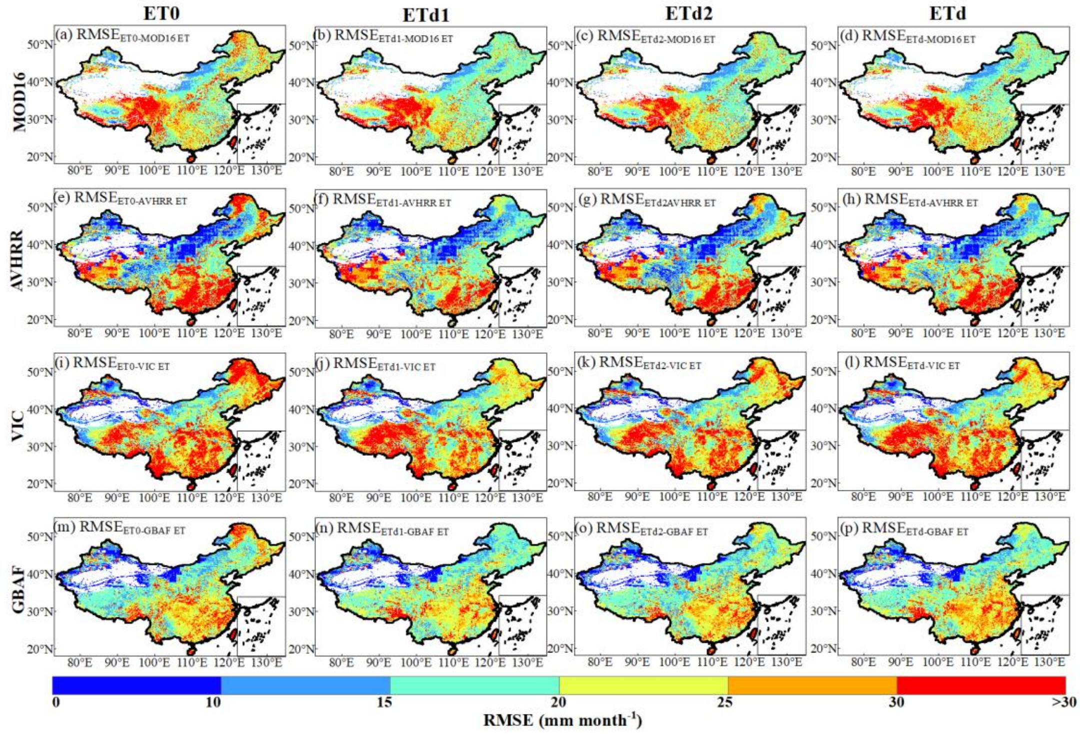

Figure 3. Maps of the RMSE between ET0, ETd1, ETd2, ETd and gridded ET products of (a–d) MOD16, (e–h) AVHRR, (i–l) VIC, and (m–p) GBAF. The per-grid RMSE between ET0, ETd1,ETd2, ETd and MOD16 (AVHRR, VIC, and GBAF) over China were computed using 156 (72, 144, and 96) samples during the period of 2001 to 2013 (2001 to 2006, 2001 to 2012, and 2001 to 2008), when the ET data are available.

5. Conclusion

The satellite-based evapotranspiration improved by revising the net incoming solar radiation via including an atmospheric emissivity algorithm and a clearness index to describe the increasing of downward longwave radiation with increasing cloudiness. The accuracy of daily net radiation routine showed good agreement with the seven ChinaFlux sites. This revised net radiation routine was incorporated into an existing satellite-based framework to convert instantaneous satellite-based observation into daily ET values. It resulted in a good fit with the evapotranspiration observed at the ChinaFlux site, a calibrated VIC hydrology model in China and three satellite-based gridded ET products in 80% percent of the area in China

Acknowledgments

Funding for this study is provided by the National Key Research and Development Program of China (No.2017YFA0603703) and the Third Xinjiang Scientific Expedition Program (No. 2021xjkk0800). The authors declare no conflicts of interest relevant to this study.

Data Availability Statement

The MODIS Land Surface Temperature/Emissivity Daily L3 Global 0.05 Deg CMG products (MOD11C1 Version 6) are available through https://lpdaac.usgs.gov/products/mod11c1v006/. The MODIS Surface Reflectance Daily L3 Global 0.05 Deg CMG products (MOD09CMG Version 6) are available through https://lpdaac.usgs.gov/products/mod09cmgv006/. The MODIS Land Cover Types Yearly L3 Global 0.05 Deg CMG products (MCD12C1 Version 6) are available through https://lpdaac.usgs.gov/products/mcd12c1v006/. The MODIS Vegetation Indices 16-Day L3 Global 0.05 Deg CMG products (MOD13C1 Version 6) are available through https://lpdaac.usgs.gov/products/mod13c1v006/. The MODIS Albedo 16-Day L3 Global 0.05 Deg CMG products (MCD43C3 Version 6) are available through https://lpdaac.usgs.gov/products/mcd43c3v006/. The radiation data set used in this study was developed by the Ministry of Education Key Laboratory for Earth System Modeling, Department of Earth System Science, Tsinghua University and the Center for Excellence in Tibetan Plateau Earth Sciences, Institute of Tibetan Plateau Research, Chinese Academy of Sciences. The radiation data is available at http://data.tpdc.ac.cn/en/data/8028b944-daaa-4511-8769-965612652c49/. The ChinaFlux data can be accessed by http://chinaflux.org/general/index.aspx?nodeid=12. Other data that supports the analysis and conclusions of this work is available at https://doi.org/10.6084/m9.figshare.18318755.

References

Alados, I., Foyo-Moreno, I., & Alados-Arboledas, L. (2012). Estimation of downwelling longwave irradiance under all-sky conditions. *International Journal of Climatology*, *32*(5), 781–793. https://doi.org/10.1002/joc.2307

Alfieri, J. G., Anderson, M. C., Kustas, W. P., & Cammalleri, C. (2017). Effect of the revisit interval and temporal upscaling methods on the accuracy of remotely sensed evapotranspiration estimates. *Hydrology and Earth System Sciences*, *21*(1), 83–98. https://doi.org/10.5194/hess-21-83-2017

Brutsaert, W. (1975). On a derivable formula for long-wave radiation from clear skies. *Water Resources Research*, *11*(5), 742–744. https://doi.org/10.1029/WR011i005p00742

Brutsaert, W., & Sugita, M. (1992). Application of self-preservation in the diurnal evolution of the surface energy budget to determine daily evaporation. *Journal of Geophysical Research: Atmospheres*, *97*(D17), 18377–18382. https://doi.org/10.1029/92JD00255

Cammalleri, C., Anderson, M. C., & Kustas, W. P. (2014). Upscaling of evapotranspiration fluxes from instantaneous to daytime scales for thermal remote sensing applications. *Hydrology and Earth System Sciences*, *18*(5), 1885–1894. https://doi.org/10.5194/hess-18-1885-2014

Chang, K., & Zhang, Q. (2019). Modeling of downward longwave radiation and radiative cooling potential in China. *Journal of Renewable and Sustainable Energy*, *11*(6), 066501. https://doi.org/10.1063/1.5117319

De Bruin, H. a. R. (1983). A Model for the Priestley-Taylor Parameter α. *Journal of Climate and Applied Meteorology*, *22*(4), 572–578. https://doi.org/10.1175/1520-0450(1983)022<0572:AMFTPT>2.0.CO;2

Goforth, M. A., Gilchrist, G. W., & Sirianni, J. D. (2002). Cloud effects on thermal downwelling sky radiance. In *Thermosense XXIV* (Vol. 4710, pp. 203–213). SPIE. https://doi.org/10.1117/12.459570

He, J., Yang, K., Tang, W., Lu, H., Qin, J., Chen, Y., & Li, X. (2020). The first high-resolution meteorological forcing dataset for land process studies over China. *Scientific Data*, *7*(1), 25. https://doi.org/10.1038/s41597-020-0369-y

Huang, L., Li, Z., Tang, Q., Zhang, X., Liu, X., & Cui, H. (2017). Evaluation of satellite-based evapotranspiration estimates in China. *Journal of Applied Remote Sensing*, *11*(2), 026019. https://doi.org/10.1117/1.JRS.11.026019

Huang, L., Steenhuis, T. S., Luo, Y., Tang, Q., Tang, R., Zheng, J., et al. (2021). Revisiting Daily MODIS Evapotranspiration Algorithm Using Flux Tower Measurements in China. *Earth and Space Science*, *8*(10), e2021EA001818. https://doi.org/10.1029/2021EA001818

Idso, S. B. (1981). A Set of Equations for Full Spectrum and 8- to 14-µm and 10.5- to 12.5-µm Thermal Radiation From Cloudless Skies. *Water Resources Research*, *17*, 295–304. https://doi.org/10.1029/WR017i002p00295

Jung, M., Reichstein, M., & Bondeau, A. (2009). Towards global empirical upscaling of FLUXNET eddy covariance observations: validation of a model tree ensemble

approach using a biosphere model. *Biogeosciences*, *6*(10), 2001–2013. https://doi.org/10.5194/bg-6-2001-2009
Jung, Martin, Reichstein, M., Ciais, P., Seneviratne, S. I., Sheffield, J., Goulden, M. L., et al. (2010). Recent decline in the global land evapotranspiration trend due to limited moisture supply. *Nature*, *467*(7318), 951–954. https://doi.org/10.1038/nature09396
Kingston, D. G., Todd, M. C., Taylor, R. G., Thompson, J. R., & Arnell, N. W. (2009). Uncertainty in the estimation of potential evapotranspiration under climate change. *Geophysical Research Letters*, *36*(20). https://doi.org/10.1029/2009GL040267
Kondo, J., Meteorology of Water Environment, 350 pp., Asakura-shoten, Tokyo, 1994.
Kondo, J., Atmospheric Science Near the Ground Surface, 324 pp., Univ. of Tokyo Press, Tokyo, 2000.
Li, S., Yu, Y., Sun, D., Tarpley, D., Zhan, X., & Chiu, L. (2014). Evaluation of 10 year AQUA/MODIS land surface temperature with SURFRAD observations. *International Journal of Remote Sensing*, *35*(3), 830–856. https://doi.org/10.1080/01431161.2013.873149
Liu, J., Zhang, J., Kong, D., Feng, X., Feng, S., & Xiao, M. (2021). Contributions of Anthropogenic Forcings to Evapotranspiration Changes Over 1980–2020 Using GLEAM and CMIP6 Simulations. *Journal of Geophysical Research: Atmospheres*, *126*(22), e2021JD035367. https://doi.org/10.1029/2021JD035367
Lu, L., Zhang, T., Wang, T., & Zhou, X. (2018). Evaluation of Collection-6 MODIS Land Surface Temperature Product Using Multi-Year Ground Measurements in an Arid Area of Northwest China. *Remote Sensing*, *10*(11), 1852. https://doi.org/10.3390/rs10111852
McNaughton, K. G., & Jarvis, P. G. (1983). Predicting effects of vegetation changes on transpiration and evaporation. *Water Deficits and Plant Growth*. Retrieved from http://agris.fao.org/agris-search/search.do?recordID=US201302611148
Miguez-Macho, G., & Fan, Y. (2021). Spatiotemporal origin of soil water taken up by vegetation. *Nature*, *598*(7882), 624–628. https://doi.org/10.1038/s41586-021-03958-6
Mu, Q., Heinsch, F. A., Zhao, M., & Running, S. W. (2007). Development of a global evapotranspiration algorithm based on MODIS and global meteorology data. *Remote Sensing of Environment*, *111*(4), 519–536. https://doi.org/10.1016/j.rse.2007.04.015
Mu, Q., Zhao, M., & Running, S. W. (2011). Improvements to a MODIS global terrestrial evapotranspiration algorithm. *Remote Sensing of Environment*, *115*(8), 1781–1800. https://doi.org/10.1016/j.rse.2011.02.019
Nishida, K., Nemani, R. R., Running, S. W., & Glassy, J. M. (2003). An operational remote sensing algorithm of land surface evaporation. *Journal of Geophysical Research: Atmospheres*, *108*(D9). https://doi.org/10.1029/2002JD002062
Pascolini-Campbell, M., Reager, J. T., Chandanpurkar, H. A., & Rodell, M. (2021). A 10 per cent increase in global land evapotranspiration from 2003 to 2019. *Nature*, *593*(7860), 543–547. https://doi.org/10.1038/s41586-021-03503-5
Prata, A. J. (1996). A new long-wave formula for estimating downward clear-sky

radiation at the surface. *Quarterly Journal of the Royal Meteorological Society*, *122*(533), 1127–1151. https://doi.org/10.1002/qj.49712253306
Rodell, M., Famiglietti, J. S., Chen, J., Seneviratne, S. I., Viterbo, P., Holl, S., & Wilson, C. R. (2004). Basin scale estimates of evapotranspiration using GRACE and other observations. *Geophysical Research Letters*, *31*(20). https://doi.org/10.1029/2004GL020873
Ryu, Y., Baldocchi, D. D., Black, T. A., Detto, M., Law, B. E., Leuning, R., et al. (2012). On the temporal upscaling of evapotranspiration from instantaneous remote sensing measurements to 8-day mean daily-sums. *Agricultural and Forest Meteorology*, *152*, 212–222. https://doi.org/10.1016/j.agrformet.2011.09.010
Sobrino, J. A., Gómez, M., Jiménez-Muñoz, J. C., & Olioso, A. (2007). Application of a simple algorithm to estimate daily evapotranspiration from NOAA–AVHRR images for the Iberian Peninsula. *Remote Sensing of Environment*, *110*(2), 139–148. https://doi.org/10.1016/j.rse.2007.02.017
Stewart, J. B., Engman, E. T., Feddes, R. A., & Kerr, Y. H. (1998). Scaling up in hydrology using remote sensing: Summary of a Workshop. *International Journal of Remote Sensing*, *19*(1), 181–194. https://doi.org/10.1080/014311698216503
Tang, Q., Peterson, S., Cuenca, R. H., Hagimoto, Y., & Lettenmaier, D. P. (2009). Satellite-based near-real-time estimation of irrigated crop water consumption. *Journal of Geophysical Research: Atmospheres*, *114*(D5). https://doi.org/10.1029/2008JD010854
Tang, R., & Li, Z.-L. (2017). An improved constant evaporative fraction method for estimating daily evapotranspiration from remotely sensed instantaneous observations. *Geophysical Research Letters*, *44*(5), 2319–2326. https://doi.org/10.1002/2017GL072621
Tang, R., Li, Z.-L., & Sun, X. (2013). Temporal upscaling of instantaneous evapotranspiration: An intercomparison of four methods using eddy covariance measurements and MODIS data. *Remote Sensing of Environment*, *138*, 102–118. https://doi.org/10.1016/j.rse.2013.07.001
Tang, R., Li, Z.-L., Sun, X., & Bi, Y. (2017). Temporal upscaling of instantaneous evapotranspiration on clear-sky days using the constant reference evaporative fraction method with fixed or variable surface resistances at two cropland sites. *Journal of Geophysical Research: Atmospheres*, *122*(2), 784–801. https://doi.org/10.1002/2016JD025975
Teuling, A. J., Van Loon, A. F., Seneviratne, S. I., Lehner, I., Aubinet, M., Heinesch, B., et al. (2013). Evapotranspiration amplifies European summer drought. *Geophysical Research Letters*, *40*(10), 2071–2075. https://doi.org/10.1002/grl.50495
Vall, S., & Castell, A. (2017). Radiative cooling as low-grade energy source: A literature review. *Renewable and Sustainable Energy Reviews*, *77*, 803–820. https://doi.org/10.1016/j.rser.2017.04.010
Van Niel, T. G., McVicar, T. R., Roderick, M. L., van Dijk, A. I. J. M., Beringer, J., Hutley, L. B., & van Gorsel, E. (2012). Upscaling latent heat flux for thermal remote sensing studies: Comparison of alternative approaches and correction of

bias. *Journal of Hydrology*, *468–469*, 35–46. https://doi.org/10.1016/j.jhydrol.2012.08.005

Wang, K., Wan, Z., Wang, P., Sparrow, M., Liu, J., & Haginoya, S. (2007). Evaluation and improvement of the MODIS land surface temperature/emissivity products using ground-based measurements at a semi-desert site on the western Tibetan Plateau. *International Journal of Remote Sensing*, *28*(11), 2549–2565. https://doi.org/10.1080/01431160600702665

Wang, Kaicun, & Dickinson, R. E. (2012). A review of global terrestrial evapotranspiration: Observation, modeling, climatology, and climatic variability. *Reviews of Geophysics*, *50*(2). https://doi.org/10.1029/2011RG000373

Wang, Kaicun, & Dickinson, R. E. (2013). Global atmospheric downward longwave radiation at the surface from ground-based observations, satellite retrievals, and reanalyses. *Reviews of Geophysics*, *51*(2), 150–185. https://doi.org/10.1002/rog.20009

Wang, Kaicun, & Liang, S. (2009a). Evaluation of ASTER and MODIS land surface temperature and emissivity products using long-term surface longwave radiation observations at SURFRAD sites. *Remote Sensing of Environment*, *113*(7), 1556–1565. https://doi.org/10.1016/j.rse.2009.03.009

Wang, Kaicun, & Liang, S. (2009b). Global atmospheric downward longwave radiation over land surface under all-sky conditions from 1973 to 2008. *Journal of Geophysical Research: Atmospheres*, *114*(D19). https://doi.org/10.1029/2009JD011800

Wang, L., Good, S. P., & Caylor, K. K. (2014). Global synthesis of vegetation control on evapotranspiration partitioning. *Geophysical Research Letters*, *41*(19), 6753–6757. https://doi.org/10.1002/2014GL061439

Xu, T., Liu, S., Xu, L., Chen, Y., Jia, Z., Xu, Z., & Nielson, J. (2015). Temporal Upscaling and Reconstruction of Thermal Remotely Sensed Instantaneous Evapotranspiration. *Remote Sensing*, *7*(3), 3400–3425. https://doi.org/10.3390/rs70303400

Yang, D., Chen, H., & Lei, H. (2013). Analysis of the Diurnal Pattern of Evaporative Fraction and Its Controlling Factors over Croplands in the Northern China. *Journal of Integrative Agriculture*, *12*(8), 1316–1329. https://doi.org/10.1016/S2095-3119(13)60540-7

Yang, K., He, J., Tang, W., Qin, J., & Cheng, C. C. K. (2010). On downward shortwave and longwave radiations over high altitude regions: Observation and modeling in the Tibetan Plateau. *Agricultural and Forest Meteorology*, *150*(1), 38–46. https://doi.org/10.1016/j.agrformet.2009.08.004

Yang, Y., Long, D., & Shang, S. (2013). Remote estimation of terrestrial evapotranspiration without using meteorological data. *Geophysical Research Letters*, *40*(12), 3026–3030. https://doi.org/10.1002/grl.50450

Yu, G.-R., Wen, X.-F., Sun, X.-M., Tanner, B. D., Lee, X., & Chen, J.-Y. (2006). Overview of ChinaFLUX and evaluation of its eddy covariance measurement. *Agricultural and Forest Meteorology*, *137*(3), 125–137. https://doi.org/10.1016/j.agrformet.2006.02.011

Zhang, K., Kimball, J. S., Mu, Q., Jones, L. A., Goetz, S. J., & Running, S. W. (2009). Satellite based analysis of northern ET trends and associated changes in the regional water balance from 1983 to 2005. *Journal of Hydrology*, *379*(1), 92–110. https://doi.org/10.1016/j.jhydrol.2009.09.047

Zhang, X.-J., Tang, Q., Pan, M., & Tang, Y. (2014). A Long-Term Land Surface Hydrologic Fluxes and States Dataset for China. *Journal of Hydrometeorology*, *15*(5), 2067–2084. https://doi.org/10.1175/JHM-D-13-0170.1

Zheng, H., Yu, G., Wang, Q., Zhu, X., He, H., Wang, Y., et al. (2016). Spatial variation in annual actual evapotranspiration of terrestrial ecosystems in China: Results from eddy covariance measurements. *Journal of Geographical Sciences*, *26*(10), 1391–1411. https://doi.org/10.1007/s11442-016-1334-8

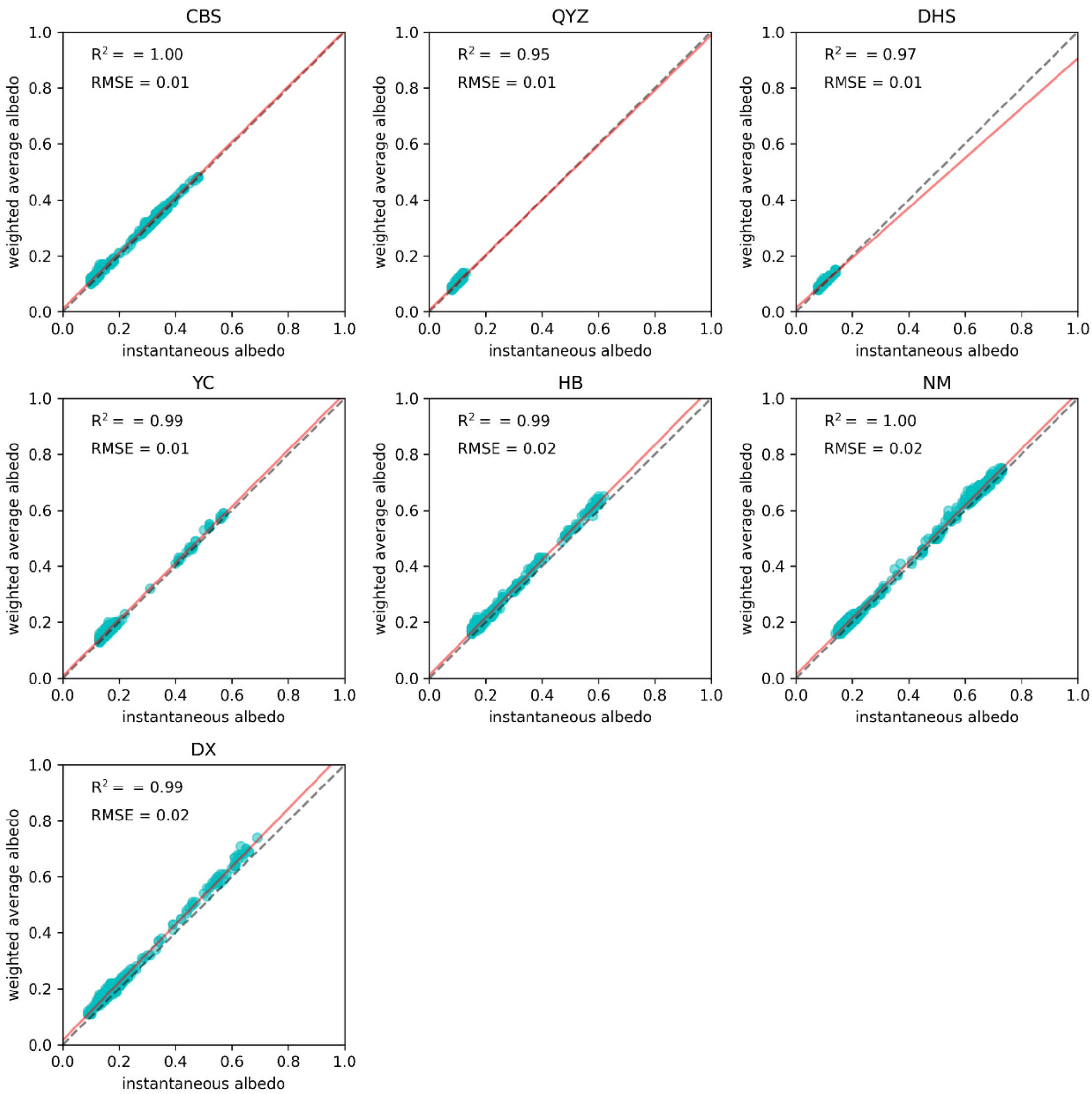

Figure S1. The comparison of instantaneous albedo and weighted daily average albedo in for the entire 2003 to 2005 period at Changbaishan (CBS), Qianyanzhou (QYZ), Dinghushan (DHS), Yucheng (YC) and Haibei (HB). 2004 to 2005 at Neimeng (NM), and Dangxiong (DX) sites. The red line is the linear fit line, the dotted line is the 1:1 line.

Table S1. The input data which include MODIS Land product and China Meteorological Forcing data used in this study. The names of these dataset, the used parameters, the time steps and the spatial resolution is shown below.

Data source	**Data name**	**Used parameter**	**Time step**	**Spatial resolution**	**Purpose**
MODIS Land Product	MOD11C1	Land Surface Temperature /Emissivity	daily	0.05 degree	Used as T_S in Eq. (15) to Calculate net radiation and Calculate air temperature with NDVI by VI-TS method
	MOD09CMG	Surface Reflectance	daily	0.05 degree	Used as ε_s in Eq. (15) to Calculate net radiation
	MCD43C3	Albedo	16-day	0.05 degree	Used as albedo in Eq. (15) to Calculate net radiation
	MOD13C1	NDVI	16-day	0.05 degree	Calculating air temperature with Ts by VI-TS method Calculating the vegetation coverage
	MCD12C1	Land cover	yearly	0.05 degree	Identifying the land surface cover to determine the parameter scheme resistances
China Meteorological Forcing Dataset	Srad	shortwave radiation	3-hourly	0.1degree	Used as R_d Eq. (15) to Calculate the net radiation

Table S2. Flux tower measurement sites with the longitudes, latitudes, altitudes, land cover types, climate types and the time period of the measurements data used.

Flux tower	Lon. (°E)	Lat. (°N)	Altitude (m)	Land cover	Footprint (m)	Climate	Time period
Changbaishan	128.1	42.4	738	Forest	181 to 3070	Monsoon temperate continental climate	2003-2005
Qianyanzhou	115.06	26.74	102	Forest	120 to 1655	Subtropical monsoon climate	2003-2005
Dinghushan	112.53	23.17	240	Forest	129 to 1908	Monsoon humid climate	2003-2005
Yucheng	116.57	36.83	28	Cropland	16 to 190	Semi-humid monsoon climate	2003-2005
Haibei	101.32	37.62	3190	Grassland	19 to 195	Plateau continental climate	2003-2005
Neimeng	116.67	43.53	1200	Grassland	19 to 195	Temperate arid and semiarid continental climate	2004-2005
Dangxiong	91.07	30.5	4350	Grassland	27 to 163	Plateau monsoon climate	2004-2005

Table S3. Four independent gridded ET products

Product name	Temporal resolution	Spatial resolution	Time period	Theory	Reference
MOD16	Monthly	1 km	2001-2013	Penman-Moteith	Mu et al (2007, 2011)
AVHRR	Monthly	1 degree	2001-2006	Priestly-Taylor	Zhang et al., (2006, 2010)
GBAF	Monthly	0.5 degree	2001-2008	Machine learning	Jung et al., (2006, 2010)
VIC	Daily	0.25 degree	2001-2012	Water balance	Zhang et al., (2014a, 2014b)

Pearson's correlation coefficient is calculated as:

$$r = \frac{\sum(X-\bar{X})(Y-\bar{Y})}{\sqrt{\sum(X-\bar{X})^2\sum(Y-\bar{Y})^2}} \qquad \text{(Equation S1)}$$

r is the Pearson's correlation coefficient; X is the estimated variable; $\bar{X}$ is the average of X; Y is the observed variable; $\bar{Y}$ is the average of Y.

Root Mean Square Error:

$$RMSE = \sqrt{\frac{\sum_{i=1}^{N}(X_i-Y_i)^2}{N}} \qquad \text{(Equation S2)}$$

$RMSE$ is the Root Mean Square Error; N is the sample size.

The relative error is calculated as:

$$RE = \frac{X-Y}{Y} \times 100\% \qquad \text{(Equation S3)}$$

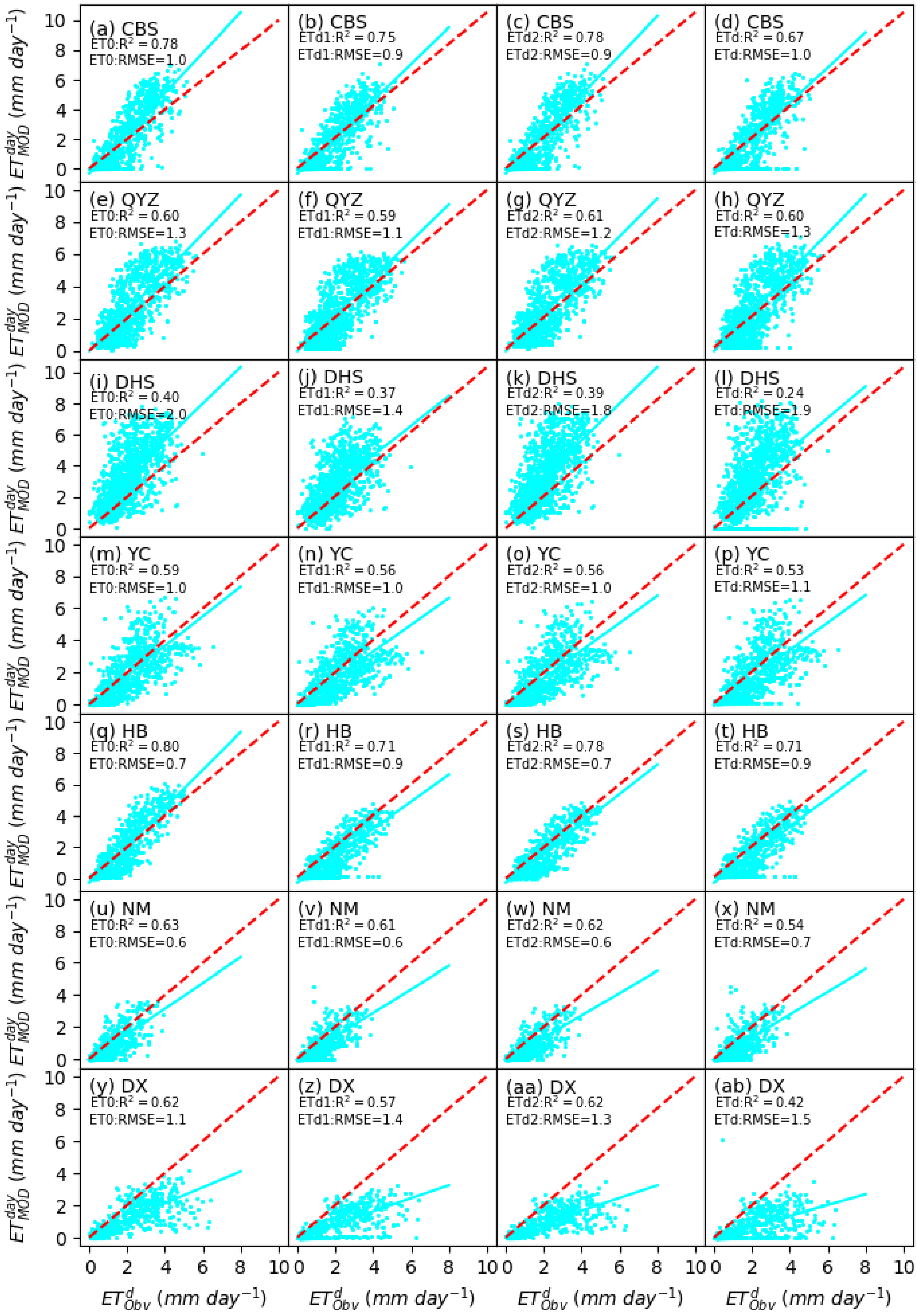

Figure S2. Scatter plots of satellite-based model simulated daily ET0, ETd1, ETd2 and ETd (the blue dots) plotted against the observed measurements ($ET^{d}{}_{Obv}$) for the entire 2003 to 2005 period at Changbaishan (CBS), Qianyanzhou (QYZ), Dinghushan (DHS), Yucheng (YC) and Haibei (HB). 2004 to 2005 at Neimeng (NM), and Dangxiong (DX) sites. The blue line is the linear fit line, the red dotted line is the 1:1 line.

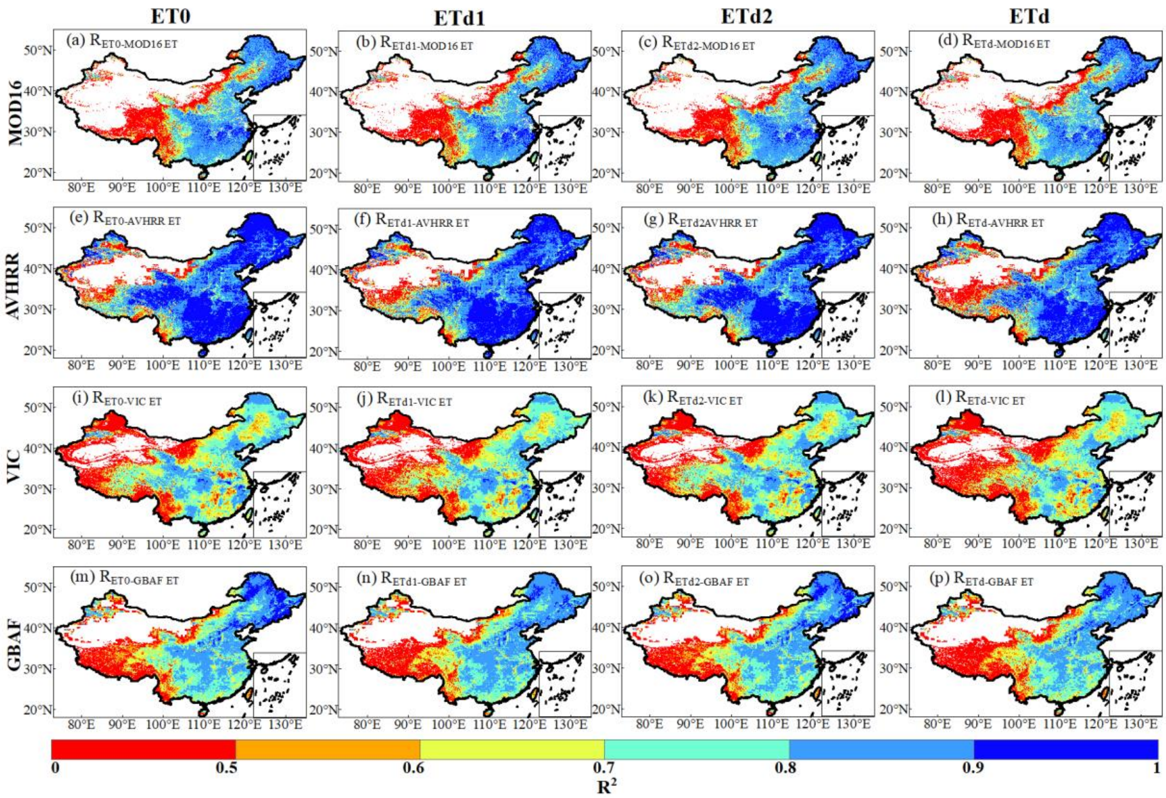

Figure S3. Maps of the R^2 between ET0, ETd1, ETd2, ETd and gridded ET products of (a–d) MOD16, (e–h) AVHRR, (i–l) VIC, and (m–p) GBAF. The per-grid R^2 between ET0, ETd1,ETd2, ETd and MOD16 (AVHRR, VIC, and GBAF) over China were computed using 156 (72, 144, and 96) samples during the period of 2001 to 2013 (2001 to 2006, 2001 to 2012, and 2001 to 2008), when the ET data are available.

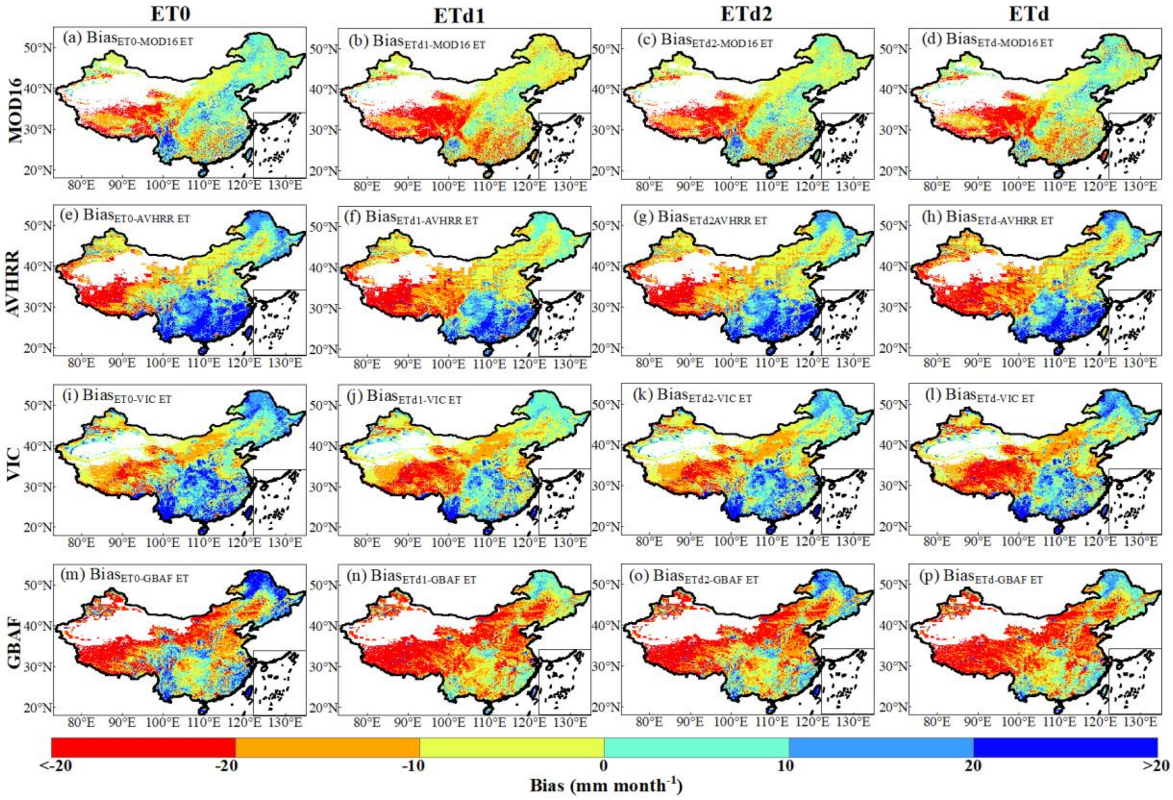

Figure S4. Maps of the bias (Bias) between ET0, ETd1, ETd2, ETd and gridded ET products of (a–d) MOD16, (e–h) AVHRR, (i–l) VIC, and (m–p) GBAF. The per-grid bias between ET0, ETd1,ETd2, ETd and MOD16 (AVHRR, VIC, and GBAF) over China were computed using 156 (72, 144, and 96) samples during the period of 2001 to 2013 (2001 to 2006, 2001 to 2012, and 2001 to 2008), when the ET data are available.